International Journal of Academic Engineering Research (IJAER)
ISSN: 2643-9085
Vol. 10 Issue 8 August - 2026, Pages: 14-22

Fabrication of electrospun PVC/PVDF blend tribo-negative layers and evaluation of their physicochemical and triboelectric properties

Nguyen Thi Thuy Duong[1,2], Le Trong Lu[2], Vu The Minh[3]

[1]Graduate University of Science and Technology, Vietnam Academy of Science and Technology, Hanoi, Viet Nam
[2]Institute for Tropical Technology, Vietnam Academy of Science and Technology, Hanoi, Viet Nam
[3]Marie Curie High School, Ho Chi Minh City, Vietnam. Email: minhvuthe173@gmail.com
* Corresponding author. E-mail: thuyduongnguyen.usth@gmail.com

Abstract: *Triboelectric nanogenerators (TENGs) convert ambient mechanical motion into electricity, but their output is bounded by the charge-accepting capacity of the tribo-negative layer. Fluorinated and chlorinated polymers are the most strongly tribo-negative commodity materials available, yet blends of the two have rarely been assessed as TENG electrodes, and the separate contribution of the shaping process has not been isolated. Here, poly(vinyl chloride)/poly(vinylidene fluoride) (PVC/PVDF) blends spanning the full composition range (0:100, 20:80, 50:50, 80:20 and 100:0 by mass) were shaped into ~50 µm layers by electrospinning and by solution casting, deposited on Cu current collectors and tested against an acrylic counter-electrode in vertical contact–separation mode. Electron microscopy showed bead-free randomly oriented fibres that were most uniform at the equimass composition, while FT-IR confirmed that blending was purely physical. Output was strongly non-monotonic in composition: the 50:50 electrospun mat delivered the highest peak-to-peak open-circuit voltage, 442 V, exceeding both neat PVDF (384 V) and neat PVC (196 V), and retained ~80% of its initial output after 10,900 cycles at 5 Hz. Electrospinning outperformed casting at every composition, by 3.43-fold for neat PVDF but by only 1.36 to 1.85-fold for the PVC-rich compositions. Each value rests on a single determination, but the pattern is consistent with a geometric contribution common to all films acting together with an additional, PVDF-specific contribution.*

Keywords: Triboelectric Nanogenerator; Polymer Blend; Electrospinning; Poly(Vinylidene Fluoride); Poly(Vinyl Chloride); Tribo-Negative Electrode

1. Introduction

Distributed sensing, wearable electronics and the Internet of Things are expanding faster than battery technology can service them, and the maintenance burden of replacing millions of small cells has made ambient energy harvesting a practical rather than an academic concern. Triboelectric nanogenerators (TENGs), introduced in 2012, convert low-frequency mechanical motion into electricity by combining contact electrification with electrostatic induction [1,2]. They are attractive because they use inexpensive materials, tolerate irregular excitation, and, unlike electromagnetic generators, become more efficient as frequency falls, which is precisely the regime of human motion, wind gusts and machinery vibration [3–5].

Because charge separation occurs at the contacting surfaces, the choice of tribo-active material sets the ceiling on device performance [6,7]. The tribo-negative side is conventionally occupied by fluoropolymers such as polytetrafluoroethylene (PTFE) and fluorinated ethylene propylene (FEP), which sit at the extreme negative end of the triboelectric series. Their dominance is nonetheless awkward in practice: PTFE is chemically inert and has very low surface energy, so it adheres poorly to current collectors and resists the surface modification used to raise charge density, and both PTFE and FEP are considerably more expensive than commodity thermoplastics [8,9]. There is therefore a clear incentive to identify tribo-negative layers that are cheaper, easier to bond to metal, and processable by scalable routes.

Poly(vinyl chloride) (PVC) is the third most produced synthetic polymer worldwide and carries a high density of strongly electron-withdrawing C–Cl bonds, yet it has been studied far less as a TENG tribo-layer than its abundance would suggest. The work that does exist has concentrated almost entirely on plasticised PVC gels, where added plasticiser raises permittivity and stretchability [10], or on recovered plastic films paired with polyamide [11]. Both strategies keep PVC in a soft, additive-laden state that is difficult to bond durably to a metal collector. Unplasticised PVC as a durable, solvent-processable tribo-negative electrode remains largely unexplored, and its inherent brittleness and thermally driven dehydrochlorination are recognised obstacles that any practical formulation must offset.

Poly(vinylidene fluoride) (PVDF) is the natural partner. Its electroactive β phase, in which the –CH_2–CF_2– units adopt an all-*trans* conformation with aligned dipoles, contributes both a high dielectric constant and a strong electron affinity, and the elongational flow and intense electric field of electrospinning are known to promote α → β conversion *in situ* [12,13]. Most reported PVDF-based TENGs, however, pursue performance by adding conductive, semiconducting or two-dimensional fillers such as graphene, MXene or metal oxides [13,14]. Filler-free blending of two commodity polymers, in which one component supplies dipolar and crystalline order while the other supplies charge-trapping

heterogeneity, has received comparatively little attention, and where blends have been examined the shaping route has usually been held constant, so morphological and compositional contributions cannot be separated.

This study addresses that gap. PVC/PVDF blends were prepared across the whole composition range and converted into tribo-negative layers of matched thickness by two routes, electrospinning and solution casting, so that composition and morphology could be varied independently within one experimental design. The films were characterised for fibre morphology, chemical structure, thermal stability and mechanical response, then assembled into contact–separation TENGs against a common acrylic counter-electrode. We report a pronounced, non-monotonic composition dependence with a maximum at the equimass blend, quantify how much of the electrospinning advantage is geometric and how much is specific to PVDF, and assess cyclic stability over ~10^4 cycles.

2. Materials and methods

2.1. Materials

PVDF (99.5%, Mw ≈ 1.0 × 10^6 g mol^{-1}) and PVC (99.8%, Mw = 2.3 × 10^5 g mol^{-1}) were obtained from a commercial supplier in China and were used as received. N,N-dimethylformamide (DMF, 99.8%), tetrahydrofuran (THF, 99.9%) and acetone (99.5%) were purchased from Sigma-Aldrich (USA). Acrylic sheet and copper foil (both 0.03 mm thick, 10 × 10 cm^2) were obtained from Macklin (China). All reagents were used as received.

2.2. Preparation of PVC/PVDF blend films

PVC and PVDF were co-dissolved at the mass ratios in a THF/DMF/acetone mixture (3:2:1 v/v) at a loading of 1 g of total polymer per 20 mL of solvent. Dissolution was carried out under magnetic stirring for 2 h at 30 °C.

Electrospun films (E). The solution was electrospun at room temperature with a needle-to-collector distance of 16 cm and a feed rate of 10 mL h^{-1}, the fibres being collected directly on copper foil. All five compositions were spun in a single session under nominally identical conditions, so that composition remained the only variable between mats.

Solution-cast films (M). The same solutions were poured into a silicone mould (10 × 10 cm^2) and dried at 50–60 °C for 24 h.

Both routes produced films of approximately 50 µm thickness, which were used without further treatment. Five compositions were prepared across the full PVC:PVDF range and are referred to throughout by the sample codes PVDF (0:100), PVC.2/PVDF.8 (20:80), PVC.5/PVDF.5 (50:50), PVC.8/PVDF.2 (80:20) and PVC (100:0), the figures in parentheses denoting the PVC:PVDF mass ratio.

2.3. Characterisation

Fibre morphology was examined by field-emission scanning electron microscopy (FE-SEM, Hitachi S-4800, Japan) after Pt sputter-coating. Infrared spectra were recorded on a Nicolet iS10 spectrometer (Thermo Fisher) over 400–4000 cm^{-1} at 8 cm^{-1} resolution with 32 scans. Thermal stability was assessed on a NETZSCH TG 209 F1 Libra analyser (Germany); TG curves were recorded for PVC, PVDF and the equimass electrospun blend PVC.5/PVDF.5. Impact resistance was measured with an Erichsen 304 ASO tester (2 kg falling ball, five repeats) following ISO 6272-1 and ASTM D2794; bending resistance was determined on an Elcometer 1500 conical mandrel according to TCVN 2099:2013; tensile strength, elastic modulus and elongation at break were obtained on a Zwick Z2.5 universal tester at 50 mm min^{-1} following ASTM D638.

2.4. TENG assembly and electrical measurement

Devices were built in vertical contact–separation mode (**Fig. 1a**). The blend film on Cu foil (10 × 10 cm^2) served as the tribo-negative electrode; an acrylic sheet on a second Cu foil served as the tribo-positive counter-electrode. The two electrodes were mounted in a 3D-printed frame and driven by a pneumatically actuated tap-and-release rig (**Fig. 1b, c**) that applied a contact force of constant magnitude at a controlled frequency. Open-circuit voltage was recorded on a LeCroy WaveSurfer oscilloscope. All compositions and both processing routes were measured under identical actuation conditions so that the comparison between them is internally consistent. Cyclic durability was evaluated at 5 Hz by comparing the peak-to-peak voltage of the first and last 200 cycles, the retained output being expressed as $\eta_v = V_n/V_0 \times 100\%$.

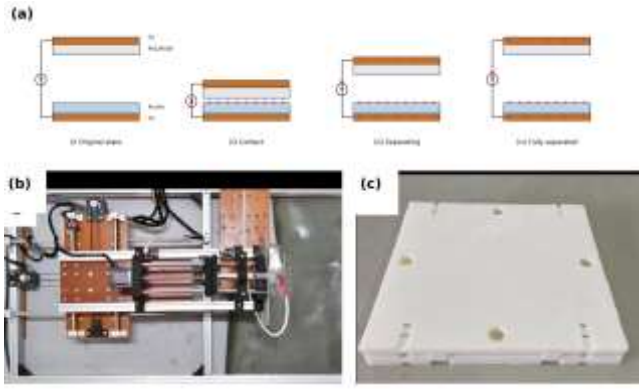

Fig. 1. (a) Working principle of the vertical contact–separation TENG built from a PVC/PVDF blend film on Cu (tribo-negative) and an acrylic layer on Cu (tribo-positive), shown through one full cycle. (b) Electrospinning rig used to deposit the fibre mats. (c) 3D-printed tap-and-release device housing the electrode pair.

3. Results

3.1. Fibre morphology

FE-SEM images of the electrospun mats (**Fig. 2**) show continuous, bead-free fibres in random three-dimensional arrangement for every composition, confirming that the mixed-solvent system supported stable jet formation across

the whole range. Neat PVDF (Fig. 2b) produced the finest and most narrowly distributed fibres, consistent with the low viscosity of its spinning dope [15], although occasional swollen, elongated segments indicate intermittent jet instability. Neat PVC (Fig. 2f) gave visibly coarser and less uniform fibres, as expected from the higher solution viscosity conferred by strong PVC–PVC chain interactions [16]. The blends were intermediate, and the equimass film PVC.5/PVDF.5 (Fig. 2d) presented the most regular fibre population and the most open, evenly distributed pore structure of the series, while the PVC-rich PVC.8/PVDF.2 mat (Fig. 2e) again showed swollen segments of the kind seen in neat PVDF. Since the viscosity argument above would predict coarse rather than swollen fibres at this composition, the defect population of the PVC-rich mat is not explained by solution viscosity alone, and no single cause is proposed here. Since the effective contact area available for charge exchange scales with the regularity and openness of the mat rather than with its projected area, this morphological optimum is the first indication that the equimass composition is electrically privileged.

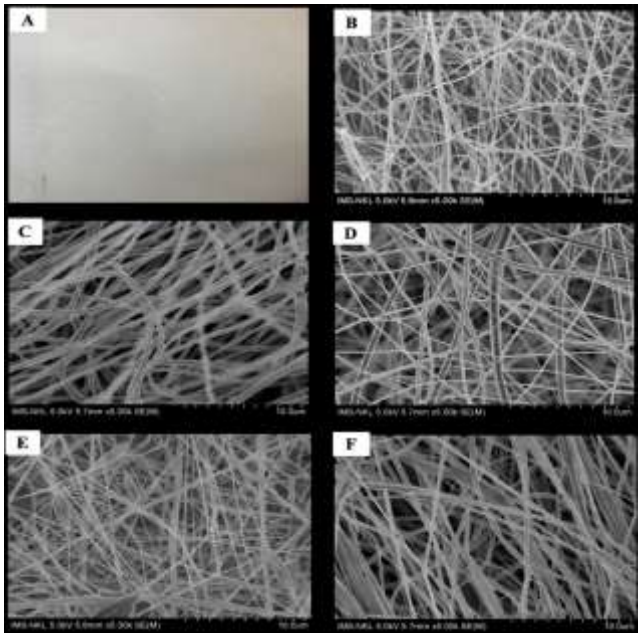

Fig. 2. (a) Photograph of an electrospun PVC/PVDF mat. FE-SEM micrographs of (b) PVDF, (c) PVC.2/PVDF.8, (d) PVC.5/PVDF.5, (e) PVC.8/PVDF.2 and (f) PVC. Scale bar 10 μm in all micrographs.

3.2. Chemical structure

FT-IR spectra (**Fig. 3**, assignments in **Table 2**) show that both components survive blending unchanged. The PVDF spectrum displays the symmetric and antisymmetric C–F stretches at 840 and 1231 cm^{-1}. The band at 840 cm^{-1} is common to both the β and γ forms and that at 1231 cm^{-1} is characteristic of the γ form, so these data identify the electroactive phase collectively rather than distinguishing β from γ; the band diagnostic of β alone, near 1275 cm^{-1}, was not resolved, and no XRD was performed. The C–H stretch of the CH_2 group appears at 3022 cm^{-1}. Neat PVC shows its own CH_2 stretch at 2911 cm^{-1} and the diagnostic C–Cl stretch at 690 cm^{-1}. The blend spectra are additive: all four marker bands appear, their relative intensities tracking the nominal mass ratio, and no new band emerges. Blending is therefore purely physical, with no covalent coupling or detectable degradation, so any change in triboelectric output must be attributed to the spatial arrangement of the two phases rather than to new chemistry.

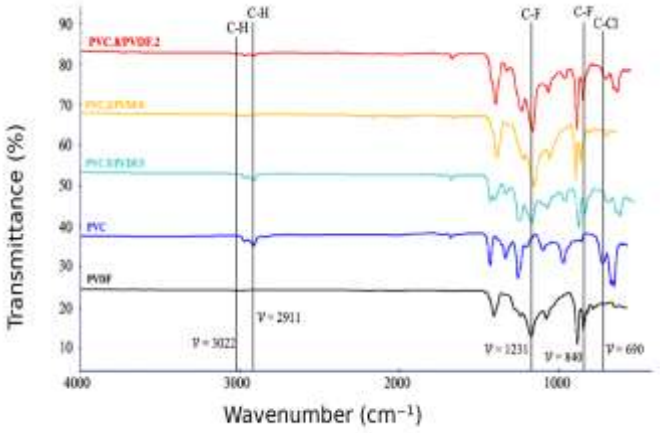

Fig. 3. FT-IR spectra of electrospun PVC/PVDF blend films across the composition range.

Table 2. Assignment of the principal FT-IR bands.

Wavenumber (cm^{-1})	Assignment	Component
3022	ν(C–H), CH_2	PVDF
2911	ν(C–H), CH_2	PVC
1231	ν_as(C–F), β/γ phase	PVDF
840	ν_s(C–F), β/γ phase	PVDF
690	ν(C–Cl)	PVC

3.3. Thermal stability

Thermogravimetric curves of PVC, PVDF and the equimass electrospun blend PVC.5/PVDF.5 (**Fig. 4**, **Table 3**) separate the three materials clearly. PVC degrades in two well-resolved steps: dehydrochlorination between about 200 and 350 °C accounts for a 61.16% mass loss, and breakdown of the residual conjugated carbon backbone between about 400 and 500 °C removes a further 27.25%, leaving roughly 12% char. PVDF is markedly more stable, losing no appreciable mass below ~420 °C and then decomposing in a single abrupt step with a 79.73% loss and ~20% residue. The equimass electrospun blend PVC.5/PVDF.5 combines the two

behaviours in a useful way: its first step is displaced upward and strongly suppressed (31.70% instead of 61.16%), its second step accounts for 44.07%, and its char residue, ~24%, is the highest of the three. PVDF thus raises the onset of PVC dehydrochlorination while PVC lowers the abruptness of PVDF breakdown, and the onset of mass loss for the blend read from the TG curve lies near 250 °C — comfortably beyond the frictional heating expected in a contact–separation device.

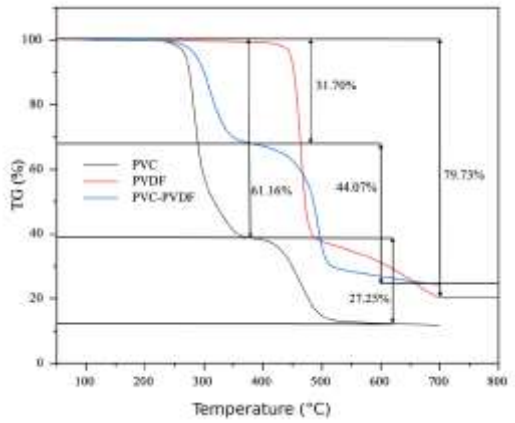

Fig. 4. TG curves of PVC, PVDF and the equimass electrospun blend PVC.5/PVDF.5, with the mass loss of each decomposition step marked.

Table 3. Mass loss determined from the TG curves of Fig. 4. Step losses are the values marked on the curves; residues are obtained by difference and are quoted to the nearest per cent.

Sample	Step 1 loss (%)	Step 2 loss (%)	Residue at 800 °C (%)
PVC	61.16	27.25	~12
PVC.5/PVDF.5 (electrospun)	31.70	44.07	~24
PVDF	79.73 (single step)	–	~20

3.4. Mechanical properties

Mechanical data for the 50 µm electrospun mats are collected in **Table 4**. Impact resistance is high and only weakly composition-dependent (95–120 kg cm), and conical-mandrel bending gave an identical 2 mm rating for every film, so blending does not compromise the flexibility or adhesion needed for a coated electrode. Tensile behaviour is more discriminating. Neat PVDF combines the highest modulus (722.33 MPa) with a tensile strength of 18.56 MPa but is brittle, failing at 2.8% strain, whereas neat PVC has by far the lowest modulus (166.01 MPa) and the greatest ductility (9.2%). Among the blends, PVC.8/PVDF.2 is mechanically the strongest — 16.11 MPa, 674.86 MPa modulus and 9.2% elongation — indicating that a minority PVDF fraction reinforces a PVC matrix effectively. The equimass blend has the lowest impact resistance of the whole series (95 kg cm) and the lowest elastic modulus of the three blends (475.82 MPa), although its tensile strength (7.41 MPa) is marginally above that of PVC.2/PVDF.8 (7.24 MPa) and of neat PVC (7.29 MPa). This combination is the expected signature of a co-continuous morphology with weak interfacial stress transfer.

Table 4. Mechanical properties of the 50 µm electrospun PVC/PVDF films.

Sample	Impact resistance (kg cm)	Bending mandrel (mm)	Tensile strength (MPa)	Elastic modulus (MPa)	Elongation at break (%)
PVDF	120	2	18.56	722.33	2.80
PVC.2/ PVDF.8	100	2	7.24	510.78	1.57
PVC.5/ PVDF.5	95	2	7.41	475.82	7.22
PVC.8/ PVDF.2	100	2	16.11	674.86	9.20
PVC	100	2	7.29	166.01	9.20

3.5. Triboelectric output: composition and processing route

Open-circuit voltage traces for the five electrospun electrodes against acrylic are shown in **Fig. 5**, and the full data set for both processing routes is given in **Table 5** and compared in **Fig. 6**. Output is markedly non-monotonic in composition. The equimass mat PVC.5/PVDF.5 is the best performer of the series, delivering V_{p-p} = 442 V (V_{max} = 294 V, V_{min} = −148 V) and exceeding both neat PVDF (384 V) and neat PVC (196 V); the ranking across the series is 50:50 > 0:100 > 80:20 > 20:80 > 100:0. Since the equimass blend outperforms both parent homopolymers, its behaviour cannot be described by a rule of mixtures and points to a genuine synergy.

The processing route matters at least as much as composition. Every solution-cast film underperformed its electrospun counterpart, but not uniformly: the enhancement factor is 3.43 for neat PVDF (384 vs 112

V), 2.53 for PVC.2/PVDF.8, 1.85 for neat PVC, 1.69 for PVC.5/PVDF.5 and only 1.36 for PVC.8/PVDF.2. The advantage of electrospinning is therefore largest for neat PVDF and falls as PVC is introduced, but the trend does not extend monotonically across the whole range: neat PVC (1.85) lies above both PVC.5/PVDF.5 (1.69) and PVC.8/PVDF.2 (1.36). Notably, the best cast film (PVC.5/PVDF.5, 262 V) still surpasses the neat cast PVDF film by a factor of 2.3, so the compositional synergy survives the loss of fibrous morphology even though its magnitude is reduced.

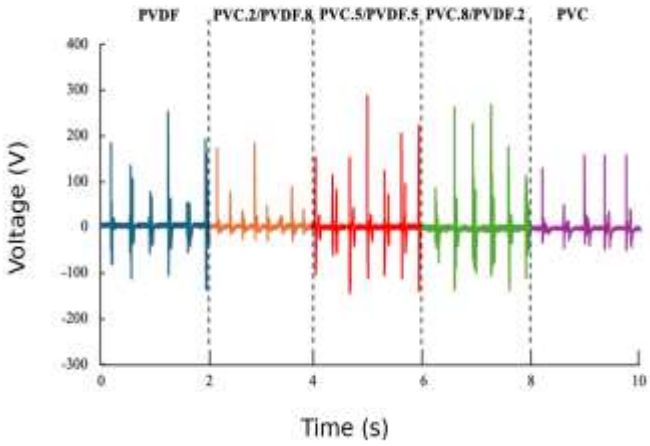

Fig. 5. Open-circuit voltage traces of the five electrospun PVC/PVDF electrodes measured against an acrylic counter-electrode under identical actuation.

Table 5. Open-circuit voltage of PVC/PVDF electrodes prepared by electrospinning (E) and solution casting (M), measured against an acrylic counter-electrode under identical actuation.

Sample	V_{max} (V), E	V_{max} (V), M	V_{min} (V), E	V_{min} (V), M	V_{p-p} (V), E	V_{p-p} (V), M	E/M
PVDF	256.0	92.0	−128.0	−20.0	384.0	112.0	3.43
PVC.2/PVDF.8	198.0	58.0	−30.0	−32.0	228.0	90.0	2.53
PVC.5/PVDF.5	294.0	186.0	−148.0	−76.0	442.0	262.0	1.69
PVC.8/PVDF.2	224.0	138.0	−106.0	−104.0	330.0	242.0	1.36
PVC	128.0	60.0	−68.0	−46.0	196.0	106.0	1.85

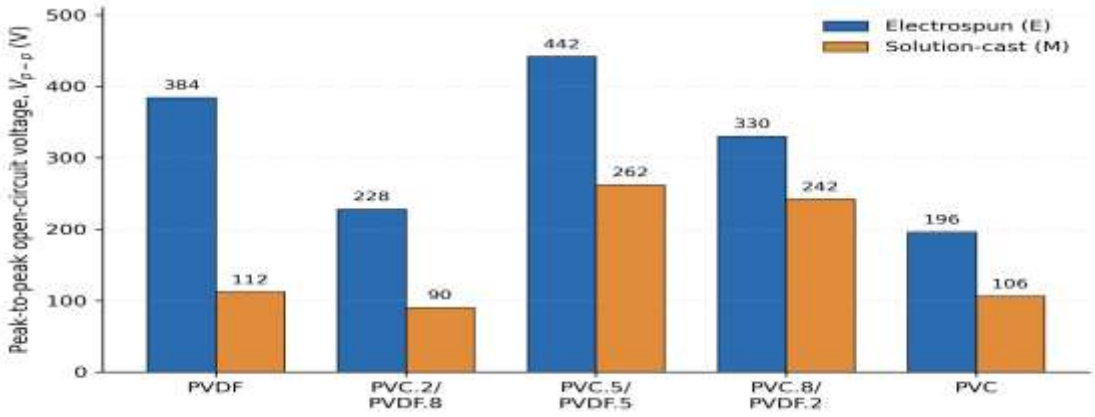

Fig. 6. Peak-to-peak open-circuit voltage of the PVC/PVDF electrodes prepared by electrospinning and by solution casting.

3.6. Cyclic durability

Because it combined the most regular fibre morphology with the highest output, PVC.5/PVDF.5 was selected for endurance testing at 5 Hz (Fig. 7). Comparing the first and last 200 cycles of a 10,900-cycle run, the device retained approximately 80% of its initial peak-to-peak voltage. The waveform remained regular and free of dropouts throughout, and no delamination from the Cu collector or visible damage to the mat was observed, so the ~20% decline reflects progressive change in the
tribo-active surface rather than mechanical failure of the electrode.

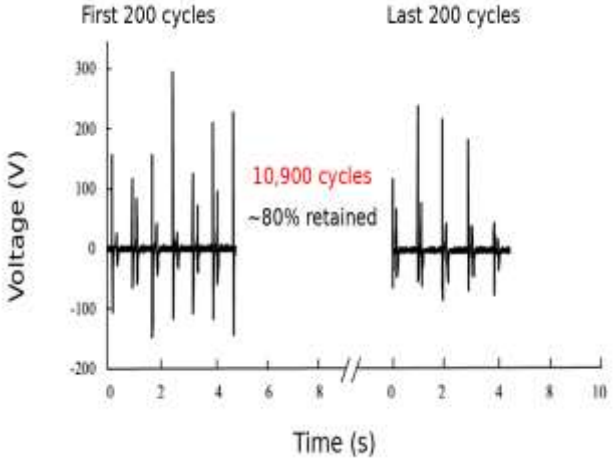

Fig. 7. Output of the PVC.5/PVDF.5 device over the first and last 200 cycles of a 10,900-cycle endurance run at 5 Hz.

4. Discussion

4.1. Origin of the compositional optimum

That the equimass blend outperforms both homopolymers requires an explanation beyond additive electron affinity, particularly since PVDF alone is the more strongly tribo-negative component. Three contributions appear to act together. First, morphology: FE-SEM shows the most regular and most open fibre population at 50:50, which maximises the number of asperities able to make and break contact per cycle and therefore the effective, as opposed to projected, contact area [17]. Second, dipolar and trap-related complementarity: the C–F bonds of PVDF supply a high permittivity and a strong electron affinity, while the C–Cl groups of PVC contribute a distinct, lower-lying set of localised electronic states. Charge injected during contact is stabilised in deep traps and the depth distribution of those traps, not surface affinity alone, governs how much charge survives to the separation half-cycle [18,19]. Third, interfacial heterogeneity: PVC and PVDF are known to interact through C–H···F and C–Cl···H dipolar contacts, giving partial miscibility and, near equimass composition, a finely divided co-continuous morphology [20]. The resulting high internal interfacial area introduces additional deep traps that impede back-flow and lateral migration of separated charge.

The mechanical data support this reading. The equimass blend has the lowest impact resistance of the series and the lowest modulus of the three blends, which is what a co-continuous morphology with limited interfacial adhesion would produce. The same fine phase texture that weakens stress transfer maximises the internal interfacial area available for
charge trapping. Optimum triboelectric output and optimum mechanical performance therefore occur at different compositions, and the two properties are effectively decoupled: charge generation is a surface and near-surface phenomenon, while stiffness and strength are bulk properties.

4.2. Why electrospinning helps, and why it helps unequally

The universal superiority of electrospun over cast films is consistent with the wider literature, where fibrous mats routinely outperform dense films of identical chemistry through greater specific surface area, intrinsic porosity, surface roughness that raises hydrophobicity and slows charge dissipation, and mechanical compliance that improves conformal contact [21,22]. What is more informative here is that the enhancement is not constant. If the benefit were purely geometric it should be similar for all compositions, since all five mats were spun under identical conditions. Instead it falls from 3.43-fold for neat PVDF through 2.53-fold and 1.69-fold to 1.36-fold for PVC.8/PVDF.2, before rising again to 1.85-fold for neat PVC. The decline across the PVDF-containing compositions is therefore clear, but the trend is not monotonic over the full range, and because each value rests on a single determination the difference between 1.36, 1.69 and 1.85 cannot be separated from measurement scatter.

The natural interpretation is that two mechanisms operate. A geometric contribution, worth roughly 1.4–1.9-fold, is common to all compositions and is the only mechanism available to PVC, which has no ferroelectric phase to orient. A second, PVDF-specific contribution comes from the strong electric field and intense elongational flow of the electrospinning jet, which are widely reported to promote the formation of the electroactive phase and to align the resulting dipoles normal to the fibre axis — an in situ ordering effect that solution casting at 50–60 °C cannot reproduce [12,13,23]. It should be noted that the present FT-IR data do not resolve the β form from the γ form, and that the electrospinning conditions were not varied, so this mechanism is inferred from the literature and from the composition dependence of the enhancement rather than demonstrated directly here. This also explains the otherwise puzzling collapse of cast PVDF to 112 V, the lowest cast value in the series: without the ordering imposed during spinning, PVDF appears to lose much of the dipolar advantage that makes it attractive. The corollary for practice is that PVC-rich blends are the more forgiving choice

when a simple casting route is required, whereas PVDF-rich formulations only realise their potential when spun.

4.3. Durability and benchmarking

compaction of the fibre mat under repeated impact, which reduces porosity and effective contact area, rather than to chemical degradation or adhesive failure. Reported approaches to this problem — crosslinking, adding a charge-trapping interlayer, or protecting the mat with a thin conformal overlayer — would be the logical next step [18,19,24].

Placed against recent work (**Table 6**), the present device is competitive given its simplicity. A filler-free blend of two commodity polymers reaching 442 V peak-to-peak over 100 cm² compares favourably with plasticised PVC-gel TENGs (24.7 V single-layer) [10] and with recycled PVC-based devices paired with polyamide (35.7 V at 5 Hz) [11]. Electrospun PVDF systems loaded with graphene reach far

Retention of ~80% after 10,900 cycles at 5 Hz, corresponding to about 36 min of continuous operation, is acceptable but not outstanding, and the absence of delamination or visible wear points to progressive

higher voltages [13], but at the cost of a conductive nanofiller, and the PVC/MXene mats that improved open-circuit voltage by 325% over neat PVC likewise depend on a two-dimensional additive [25]. The result here is closer in spirit to the electrospun PVDF/polystyrene blend of Luo et al., which raised open-circuit voltage 2.88-fold over neat PVDF by blending alone [26]. It should be stated plainly that the values in Table 6 are not strictly commensurable: devices differ in electrode area, counter-electrode material, contact force and drive frequency, and several sources report peak rather than peak-to-peak voltage — for PVC.5/PVDF.5 the corresponding peak value is 294 V, not 442 V. The comparison establishes that the material is in a useful performance class, not that it is superior.

Table 6. Comparison with recently reported polymer-based TENGs. Values are as reported by the original authors; measurement conditions differ between studies.

Tribo-negative material	Route	Counter-electrode	Output	Ref.
PVDF/graphene nanosheet	Electrospinning	–	~1511 V; ~130.2 W m^{-2}	[13]
PVDF/polystyrene	Electrospinning	–	2.88× V_oc of neat PVDF	[26]
PVC/MXene	Electrospinning	Aluminium	+325% V_oc, +490% I_sc vs neat PVC	[25]
Plasticised PVC gel (single layer)	Casting	–	24.7 V; 0.83 µA	[10]
Recycled PVC film	Commercial film	Polyamide	35.7 V; 5.85 µA at 5 Hz	[11]
PVC.5/PVDF.5 (this work)	Electrospinning	Acrylic	442 V p-p (294 V peak); 80% after 10,900 cycles	–

5. Limitations

Several constraints qualify these conclusions and define the work still required. (i) Only open-circuit voltage was measured. Short-circuit current, transferred charge and the load-resistance sweep needed to extract matched impedance and power density were not acquired, so the device cannot be ranked on power. (ii) The applied electrospinning voltage, needle gauge and ambient humidity were not recorded, and fibre diameter distributions were not quantified from the FE-SEM images; the morphological argument in Section 4.1 is therefore qualitative. (iii) The β-phase fraction was inferred from the presence of the 840 and 1231 cm^{-1} bands but not quantified by spectral deconvolution, and no XRD or DSC data were collected, so crystallinity and the degree of PVC/PVDF miscibility remain inferential. (iv) TGA was performed only on PVC, PVDF and the equimass electrospun blend; the remaining compositions were not measured, and step losses were read from the plotted curves rather than from the instrument data file, so residues quoted by difference carry an uncertainty of roughly ±1%. (v) Contact force and separation distance were held constant but not reported numerically, and all electrical data were taken at a single frequency, so the frequency dependence of the output is unknown. (vi) Surface potential (for example by Kelvin probe force microscopy), surface charge density and dielectric permittivity were not measured, leaving the trap-based mechanism proposed in Section 4.1 supported by indirect evidence only. (vii) Durability was assessed for one composition, at one frequency, for ~10^4 cycles, without humidity or temperature control; PVC is susceptible to photo- and thermo-dehydrochlorination, and long-term ageing was not evaluated. (viii) Measurements were single determinations without replicates, so no uncertainty estimates

or significance tests can be given. (ix) Performance was assessed against acrylic only; pairing against a standard PTFE or FEP counter-electrode would place the material more firmly within the triboelectric series.

6. Conclusion

PVC/PVDF blends were prepared over the full composition range and shaped into ~50 µm tribo-negative electrodes by electrospinning and by solution casting, allowing composition and morphology to be varied independently within a single experimental design. FT-IR confirmed that blending is purely physical, and thermogravimetry showed that the blend inherits a suppressed first decomposition step from PVDF and a raised char residue (~24%), extending useful thermal stability beyond that of PVC alone. Triboelectric output proved strongly non-monotonic in composition: the equimass electrospun mat PVC.5/PVDF.5 delivered 442 V peak-to-peak against acrylic, exceeding both neat PVDF (384 V) and neat PVC (196 V), and therefore not described by a rule of mixtures. This synergy is attributed to the coincidence of the most regular fibre morphology, complementary C–F and C–Cl charge-trapping states, and a finely divided co-continuous phase structure that maximises internal interfacial area — the same structure that gives this composition the lowest impact resistance of the series and the lowest modulus of the three blends, showing that charge generation and bulk mechanical performance are effectively decoupled. Electrospinning outperformed casting at every composition, but by 3.43-fold for neat PVDF and by only 1.36 to 1.85-fold for the PVC-rich compositions, which is consistent with a geometric contribution common to all films acting together with an additional, PVDF-specific contribution tentatively attributed to ordering of the electroactive phase during spinning. The optimised electrode retained ~80% of its output after 10,900 cycles at 5 Hz. A filler-free blend of two commodity polymers therefore offers a scalable, low-cost route to tribo-negative electrodes, with power characterisation and charge-retention engineering the clear next priorities.

References

[1] F.-R. Fan, Z.-Q. Tian, and Z. L. Wang, "Flexible triboelectric generator," Nano Energy, vol. 1, no. 2, pp. 328-334, 2012, doi: 10.1016/j.nanoen.2012.01.004.

[2] F.-R. Fan, L. Lin, G. Zhu, W. Wu, R. Zhang, and Z. L. Wang, "Transparent triboelectric nanogenerators and self-powered pressure sensors based on micropatterned plastic films," Nano Lett., vol. 12, no. 6, pp. 3109-3114, 2012, doi: 10.1021/nl300988z.

[3] J. Luo and Z. L. Wang, "Recent progress of triboelectric nanogenerators: From fundamental theory to practical applications," *EcoMat*, 2020, doi: 10.1002/eom2.12059.

[4] S. Niu and Z. L. Wang, "Theoretical systems of triboelectric nanogenerators," Nano Energy, vol. 14, pp. 161-192, 2015, doi: 10.1016/j.nanoen.2014.11.034.

[5] S. Niu, S. Wang, L. Lin, Y. Liu, Y. S. Zhou, Y. Hu, and Z. L. Wang, "Theoretical study of contact-mode triboelectric nanogenerators as an effective power source," Energy Environ. Sci., vol. 6, no. 12, pp. 3576-3583, 2013, doi: 10.1039/C3EE42571A.

[6] C. Xu, Y. Zi, A. C. Wang, H. Zou, Y. Dai, X. He, P. Wang, Y. C. Wang, P. Feng, D. Li, and Z. L. Wang, "On the electron-transfer mechanism in the contact-electrification effect," Adv. Mater., vol. 30, no. 15, art. no. 1706790, 2018, doi: 10.1002/adma.201706790.

[7] R. Walden, C. Kumar, D. M. Mulvihill, and S. C. Pillai, "Opportunities and challenges in triboelectric nanogenerator (TENG) based sustainable energy generation technologies: A mini-review," Chem. Eng. J. Adv., vol. 9, art. no. 100237, 2022, doi: 10.1016/j.ceja.2021.100237.

[8] Y. Wang, Y. Yang, and Z. L. Wang, "Triboelectric nanogenerators as flexible power sources," *npj Flexible Electronics*, vol. 1, Art. no. 10, Nov. 2017.

[9] J. Yang, J. Chen, Y. Liu, W. Yang, Y. Su, and Z. L. Wang, "Triboelectrification-based organic film nanogenerator for acoustic energy harvesting and self-powered active acoustic sensing," ACS Nano, vol. 8, no. 3, pp. 2649-2657, 2014, doi: 10.1021/nn4063616.

[10] H. Park, S.-J. Oh, D. Kim, M. Kim, C. Lee, H. Joo, I. Woo, J. W. Bae, and J.-H. Lee, "Plasticized PVC-Gel Single Layer-Based Stretchable Triboelectric Nanogenerator for Harvesting Mechanical Energy and Tactile Sensing," *Adv. Sci.*, May 2022, doi: 10.1002/advs.202201070.

[11] X. Feng, Q. Li, and K. Wang, "Waste plastic triboelectric nanogenerators using recycled plastic bags for power generation," ACS Appl. Mater. Interfaces, vol. 13, no. 1, pp. 400-410, 2021, doi: 10.1021/acsami.0c16489.

[12] J. Li, Q. Meng, W. Li, and Z. Zhang, "Influence of Crystalline Properties on the Dielectric and Energy Storage Properties of Poly(vinylidene fluoride)," *Journal of Applied Polymer Science*, vol. 122, no. 3, pp. 1659–1668, Nov. 2011, doi: 10.1002/app.34020.

[13] L. Shi, H. Jin, S. Dong, S. Huang, H. Kuang, H. Xu, J. Chen, W. Xuan, S. Zhang, S. Li, X. Wang, and J. Luo, "High-performance triboelectric nanogenerator based on electrospun PVDF-graphene nanosheet composite nanofibers for energy harvesting," Nano Energy, vol. 80, art. no. 105599, 2021, doi: 10.1016/j.nanoen.2020.105599.

[14] M. Kim, D. Park, M. M. Alam, S. Lee, P. Park, and J. Nah, "Remarkable output power density enhancement of triboelectric nanogenerators via polarized ferroelectric polymers and bulk MoS2 composites," ACS Nano, vol. 13, no. 4, pp. 4640-4646, 2019, doi: 10.1021/acsnano.9b00750.

[15] Q. Li, Z.-L. Xu, and L.-Y. Yu, "Effects of Mixed Solvents and PVDF Types on Performances of PVDF Microporous Membranes," *Journal of Applied Polymer Science*, vol. 115, no. 4, pp. 2277–2287, Feb. 2010, doi: 10.1002/app.31324.

[16] Y. Haiyang, Z. Pingping, L. Guofeng, W. Peng, and R. Feng, "Investigations on the intrinsic viscosity of

poly(vinyl chloride) (PVC) affected by polymer-polymer interactions in solution," Eur. Polym. J., vol. 35, no. 2, pp. 345-353, 1999, doi: 10.1016/S0014-3057(98)00136-8.

[17] H.-Y. Mi, X. Jing, Q. Zheng, L. Fang, H.-X. Huang, L.-S. Turng, and S. Gong, "High-performance flexible triboelectric nanogenerator based on porous aerogels and electrospun nanofibers for energy harvesting and sensitive self-powered sensing," *Nano Energy*, vol. 48, pp. 327–336, Jun. 2018, doi: 10.1016/j.nanoen.2018.03.050.

[18] Z. Wang, L. Cheng, Y. Zheng, Y. Qin, and Z. L. Wang, "Enhancing the performance of triboelectric nanogenerator through prior-charge injection and its application on self-powered anticorrosion," Nano Energy, vol. 10, pp. 37-43, 2014, doi: 10.1016/j.nanoen.2014.08.017.

[19] J. Zhang, Y. Zheng, L. Xu, and D. Wang, "Oleic-acid enhanced triboelectric nanogenerator with high output performance and wear resistance," Nano Energy, vol. 69, art. no. 104435, 2020, doi: 10.1016/j.nanoen.2019.104435.

[20] A. Konjarla, T. Sreekanth, A. Mallikarjun, M. R. Mettu, and M. J. Reddy, "Membrane formation of PVC and PVDF-HFP polymer blend," Mater. Today Proc., vol. 92, pp. 561-564, 2023, doi: 10.1016/j.matpr.2023.03.777.

[21] W. Zeng, L. Shu, Q. Li, S. Chen, F. Wang, and X.-M. Tao, "Fiber-based wearable electronics: A review of materials, fabrication, devices, and applications," Adv. Mater., vol. 26, no. 31, pp. 5310-5336, 2014, doi: 10.1002/adma.201400633.

[22] M.-L. Seol, J.-W. Han, D.-I. Moon, and M. Meyyappan, "Hysteretic behavior of contact force response in triboelectric nanogenerator," Nano Energy, vol. 32, pp. 408-413, 2017, doi: 10.1016/j.nanoen.2016.12.055.

[23] S. Chen, K. Yao, F. E. H. Tay, and L. L. S. Chew, "Comparative investigation of the structure and properties of ferroelectric poly(vinylidene fluoride) and poly(vinylidene fluoride-trifluoroethylene) thin films crystallized on substrates," J. Appl. Polym. Sci., vol. 116, no. 6, pp. 3331-3337, 2010, doi: 10.1002/app.31824.

[24] W. He, S. Li, P. Bai, D. Zhang, L. Feng, L. Wang, X. Fu, H. Cui, X. Ji, and R. Ma, "Multifunctional triboelectric nanogenerator based on flexible and self-healing sandwich structural film," Nano Energy, vol. 96, art. no. 107109, 2022, doi: 10.1016/j.nanoen.2022.107109.

[25] L. Liu, W. Zhu, H. Ma, and J. Zhou, "PVC/MXene electrospun film triboelectric nanogenerator for efficient mechanical energy harvesting and multifunctional human motion sensing," APL Mater., vol. 13, no. 1, art. no. 011117, 2025, doi: 10.1063/5.0245268.

[26] C. Luo, Y. Shao, H. Yu, H.-Z. Ma, Y.-H. Zhang, L. Gu, B. Yin, and M.-B. Yang, "Preparation and application of high performance PVDF/PS electrospinning film-based triboelectric nanogenerator," *Chemical Physics Letters*, vol. 813, Art. no. 140276, Feb. 2023, doi: 10.1016/j.cplett.2022.140276.